# Supplementary Material for Structures and Free Energy Landscapes of Aqueous Zinc(II)-Bound Amyloid-β(1-40) and Zinc(II)-Bound Amyloid-β(1-42) with Dynamics

*Olivia Wise-Scira*[1], *Liang Xu*[1], *George Perry*[2], and *Orkid Coskuner*[1,2]*

[1]Department of Chemistry, and [2]Neurosciences Institute, The University of Texas at San Antonio, One UTSA Circle, San Antonio, Texas 78249

Email: orkid.coskuner@utsa.edu

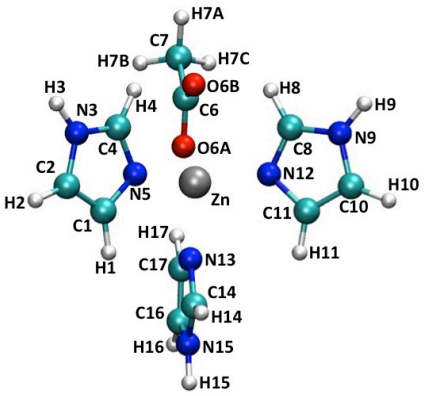


**Figure S1.** Optimized structure of the Zn:$His_3Glu$ model structure using the B3LYP functional along with the 6-31G* basis set. Each of the atoms are labeled according to the atom names used for the parameters in Table 1.

| Atom | Partial Charges | Bond Distance/Å | Calculated | Experiment |
|---|---|---|---|---|
| C1 | 0.022 | r(Zn-N5) | 2.0 | 2.1 |
| H1 | 0.119 | r(Zn-O6A) | 2.0 | 2.1 |
| C2 | -0.197 | r(Zn-O6B) | 2.4 | 2.1 |
| H2 | 0.210 | r(Zn-N12) | 2.0 | 2.2 |
| N3 | -0.177 | r(Zn-N13) | 2.1 | 2.3 |
| H3 | 0.341 | **Bond Angle/Degrees** | **Calculated** | **Experiment** |
| C4 | 0.109 | θ(Zn-O6B-C6) | 80.8 | 85.1 |
| H4 | 0.118 | θ(Zn-N12-C8) | 122.5 | 125.0 |
| N5 | -0.302 | θ(Zn-N12-C11) | 130.8 | 126.5 |
| C6 | 0.626 | θ(Zn-N13-C14) | 134.5 | 126.4 |
| O6A | -0.502 | θ(Zn-N13-C17) | 119.0 | 124.5 |
| O6B | -0.502 | θ(Zn-N5-C4) | 122.6 | 122.0 |
| C7 | -0.459 | **Torsional Angle/Degrees** | **Calculated** | **Experiment** |
| H7A | 0.139 | ϕ(Zn-N5-C1-H1) | 1.5 | -3.5 |
| H7B | 0.139 | ϕ(Zn-N5-C1-C2) | -177.6 | 176.5 |
| H7C | 0.139 | ϕ(Zn-O6A-C6-C7) | -180.0 | -177.4 |
| C8 | 0.109 | ϕ(Zn-O6B-C6-C7) | 180.0 | 177.4 |
| H8 | 0.118 | ϕ(Zn-N12-C8-H8) | 1.0 | 8.6 |
| N9 | -0.179 | ϕ(Zn-N12-C8-N9) | -177.8 | -171.4 |
| H9 | 0.341 | ϕ(Zn-N12-C11-H11) | -1.7 | -8.8 |
| C10 | -0.197 | ϕ(Zn-N12-C11-C10) | 177.5 | 171.2 |
| C11 | 0.022 | **Energy/Hartree** | -2685.97 | |
| H11 | 0.119 | | | |
| N12 | -0.302 | | | |
| N13 | -0.302 | | | |
| C14 | 0.109 | | | |
| H14 | 0.118 | | | |
| N15 | -0.179 | | | |
| H15 | 0.341 | | | |
| C16 | -0.197 | | | |
| H16 | 0.210 | | | |
| C17 | 0.022 | | | |
| H17 | 0.119 | | | |
| Zn | 0.695 | | | |

**Table S1.** Calculated specific structural parameters, electrostatic partial charges and energy of the model Zn:$His_3$Glu metal-ligand moiety with the B3LYP/6-31G*//B3LYP/6-31G* method.

The enthalpic contribution to $G$ is calculated by the sum of the molecular mechanics potential energy and the solvation free energy ($G_{sol}$), which is composed of the solvation-electrostatic free energy ($G_{sol\text{-}elec}$) and non-polar free energy ($G_{np}$) terms. For the $G_{sol\text{-}elec}$ term calculations, the internal and external dielectric constant values were set to 1 and 80, respectively and dipolar boundary conditions were applied. The $G_{np}$ contribution was calculated using the solvent accessible surface area (SASA) as shown in equation 1.

$$G_{np} = 0.00542 \times SASA + 0.92 \qquad (1)$$

Most recently, we applied both harmonic and quasi-harmonic entropy calculation methods on Aβ in an aqueous medium. The same thermodynamic trends were obtained using these different methods.[62] Therefore, the widely-used normal mode analysis method was utilized to approximate the conformational entropy values of the full-length disordered metallopeptides. For the calculations of the PMF surfaces, we used the coordinates of the end-to-end distance ($R_{E\text{-}E}$) that is defined as the distance between the Asp1 peptide backbone N-atom and the Val40 or Ala42 peptide backbone carbonyl C-atom and the radius of gyration ($R_g$). The PMF values were then calculated using equation 2.

$$PMF = -k_B T \log(P) \qquad (2)$$

where $k_B$ is the Boltzman constant and $T$ is the physiological temperature, and $P$ is the probability of Zn:Aβ structures with ceratin $R_{E\text{-}E}$ and $R_g$ values within 1 $k_B T$ range. More details can be found in Ref. 62. The convergence was verified by calculating the PMF surfaces at different simulation time-scales (see Supplementary Materials section).

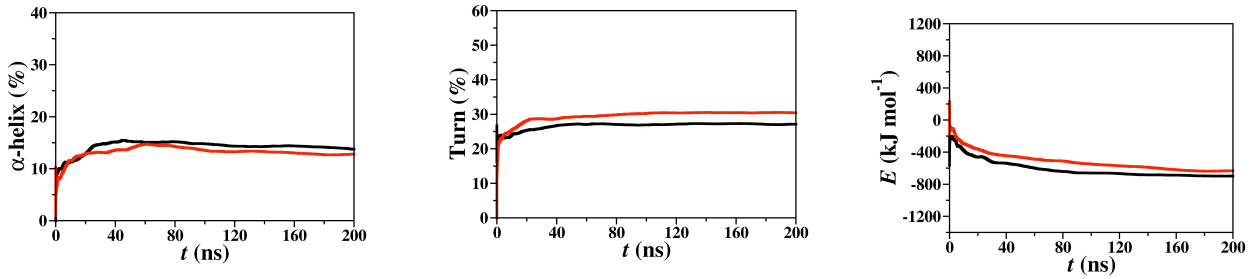


(a) (b) (c)

**Figure S2.** The calculated average (a) α-helix and (b) turn contents and the (c) internal energy ($E$) values with time using the simulated Zn:Aβ40 (black) and Zn:Aβ42 (red) metallopeptide structures in an aqueous medium.

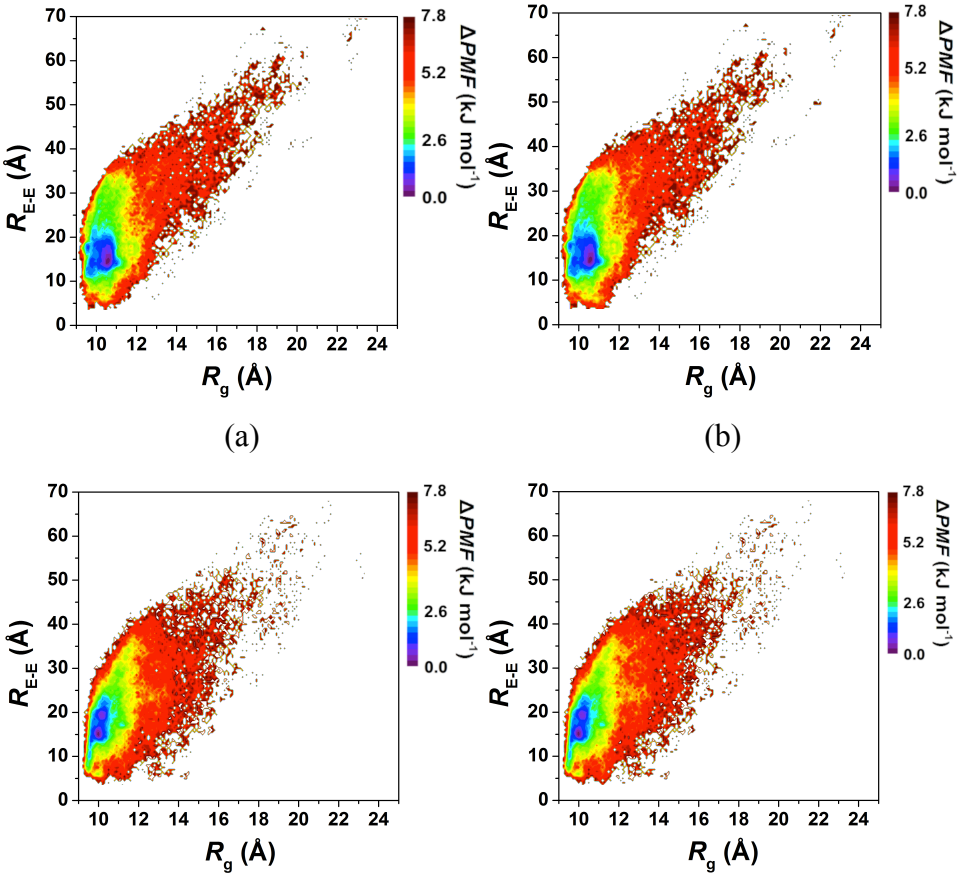


**Figure S3.** The calculated PMF surfaces based on the $R_{E-E}$ and $R_g$ values of the Zn:Aβ40 metallopeptide using the structures from the first (a) 150 ns and (b) 175 ns and the Zn:Aβ42 peptide using the structures from the first (a) 150 ns and (b) 175 ns of the simulations.

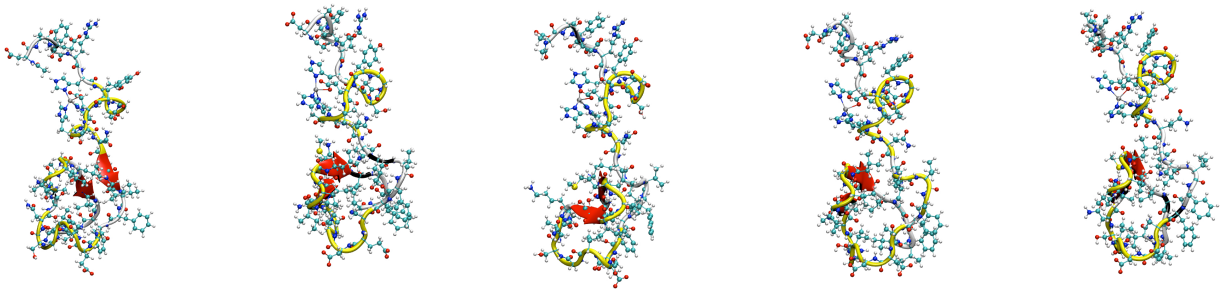


**Figure S4.** Zn:Aβ40 structures (N-terminal extended into the solution) obtained from classical molecular dynamics simulations in explicit water starting from an extended structure at (a) 0 ns, (b) 20 ns, (c) 30 ns, (d) 40 ns and (e) 50 ns. The colors on the backbone of each structures correspond to the secondary structure of each residue as follows: α-helix (blue), $3_{10}$-helix (gray), π-helix (purple), β-sheet (red), β-strand (black), turn (yellow), coil (white).

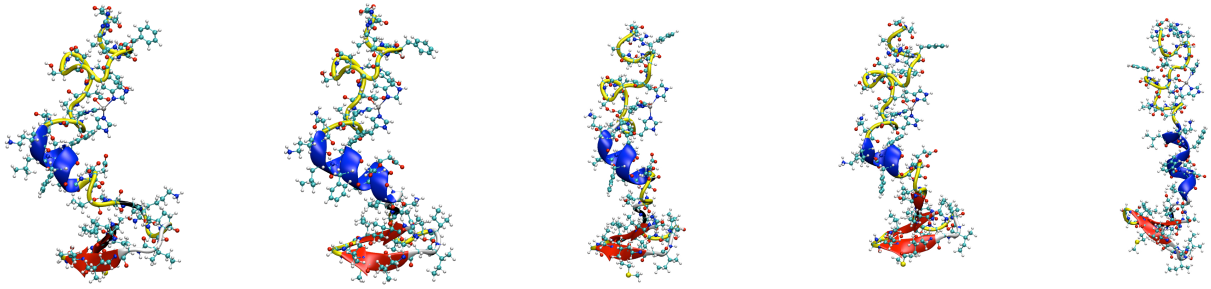

(a) (b) (c) (d) (e)

**Figure S5.** Zn:Aβ42 structures (N-terminal extended into the solution) obtained from classical molecular dynamics simulations in explicit water starting from an extended structure at (a) 0 ns, (b) 20 ns, (c) 30 ns, (d) 40 ns and (e) 50 ns. The colors on the backbone of each structures correspond to the secondary structure of each residue as follows: α-helix (blue), $3_{10}$-helix (gray), π-helix (purple), β-sheet (red), β-strand (black), turn (yellow), coil (white).

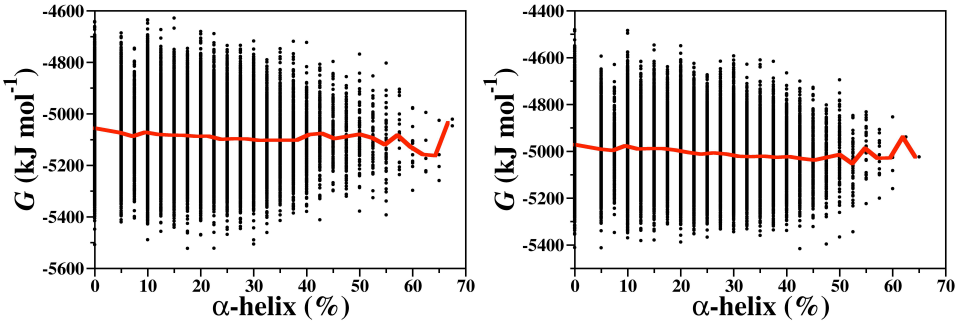


(a) (b)

**Figure S6.** The simulated α-helix abundance and associated Gibbs free energies (*G*) in the structures of the (a) Zn:Aβ40 and (b) Zn:Aβ42 metallopeptides. The red lines on the graph show the average *G* for the structures with each α-helix percentage. No clear trend is obtained between the α-helix abundance and conformational *G* values.

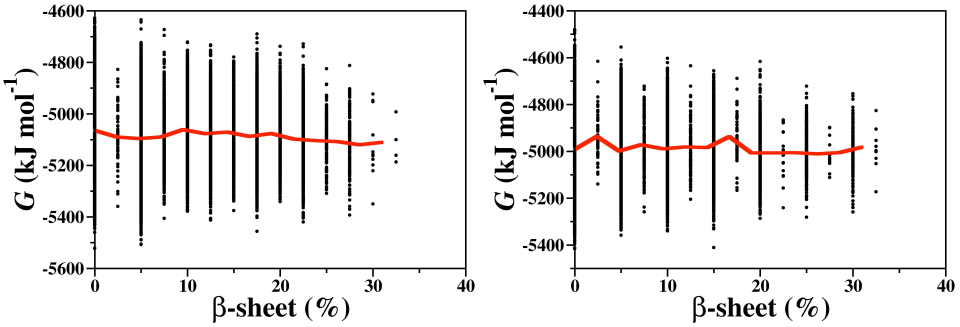


(a) (b)

**Figure S7.** The simulated β-sheet abundance and associated Gibbs free energies (*G*) in the structures of the (a) Zn:Aβ40 and (b) Zn:Aβ42 metallopeptides. The red lines on the graph show the average *G* for the structures with each β-sheet percentage. No clear trend is obtained between the β-sheet abundance and the conformational *G* values.

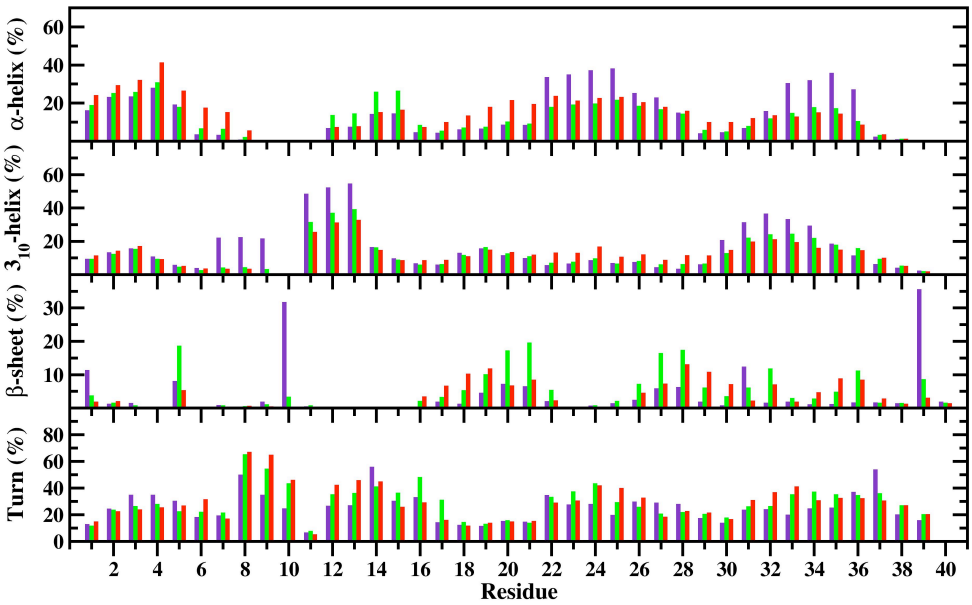


**Figure S8.** Secondary structures per residue along with their probabilities for each basin on the PMF surface of the Zn:Aβ40 metallopeptide; basin I (purple), basin II (green), and basin III (red). The abundances for the π-helix and coil structures are not displayed.

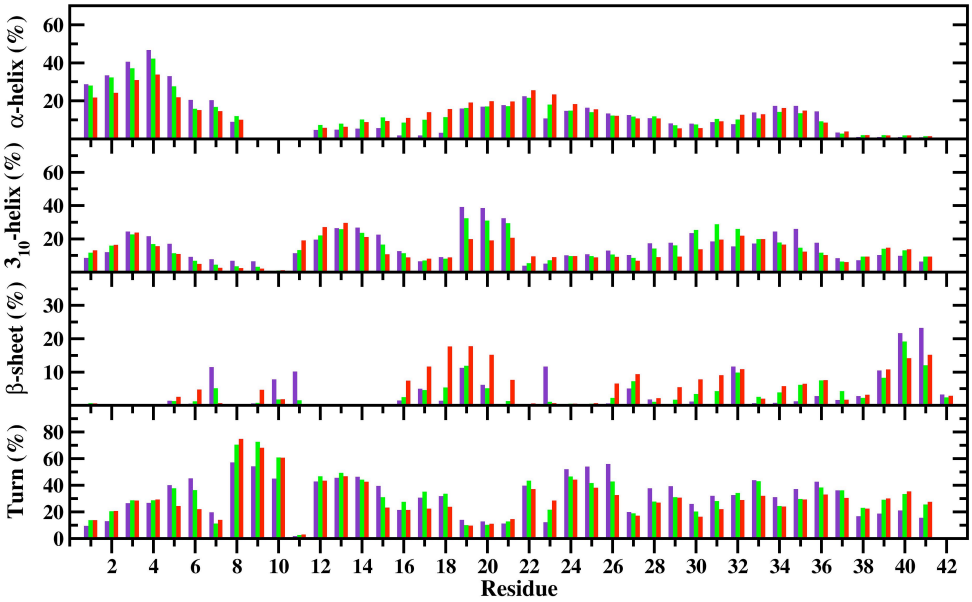

**Figure S9.** Secondary structures per residue along with the corresponding probability for each basin on the PMF surface of the Zn:Aβ42 metallopeptide; basin I (purple), basin II (green), and basin III (red). The abundances for the π-helix and coil structures are not displayed.

A direct relationship between the secondary structure abundances and conformational Gibbs free energy values could not be established for either metallopeptide without using a structural classification method. Using the PMF surfaces, we find that the helix abundance in the Zn:Aβ40 structures located in basin I is 28% and 32% larger than those located in basins II and III, respectively. This result might indicate that the Zn:Aβ40 structures become more preferred with larger helix formation. Utilizing the PMF surface, a trend in helix formation and PMF is obtained for Zn:Aβ42; structures located in basins I possess 34% and 58% larger helix abundance than those located in basins II and III, respectively. The β-sheet abundance in the structures of Zn:Aβ42 located in basin I is 11% and 34% larger than in the conformations located in basins II and III, respectively. This finding indicates that an increase both in helix and β-sheet formation stabilizes the PMF of the Zn:Aβ42 structures, which in turn might be related to the larger entropic contribution in the conformational thermodynamic stability of Zn:Aβ42 rather than Zn:Aβ40 (see above).Detailed analysis shows that the α-helix abundance is 7% - 18% larger in the mid-domain (Glu22-Gly25) and C-terminal (Gly33-Val36) regions of Zn:Aβ40 for the structures located in basin I rather than those located in basins II and III (Figure 8). Moreover, $3_{10}$-helix formation at Asp7-Gly9 and Glu11-His13 is more stable in the Zn:Aβ40 structures located in basin I rather than in those located in basins II and III. For Zn:Aβ42, there is a trend between α-helix and decreasing PMF for the residues located in the N-terminal region (Figure 9). Moreover, residues Phe19-Ala21 and Leu34-Val36 adopt more abundant $3_{10}$-helix structure in the Zn:Aβ42 conformations located in basin I rather than those located in basins II and III. Residues Asp7, Tyr10, Glu11, Asp23, Val40 and Ile41 of Zn:Aβ42 are capable of adopting prominent β-sheet structure with more favorable PMF values (Figure 9).

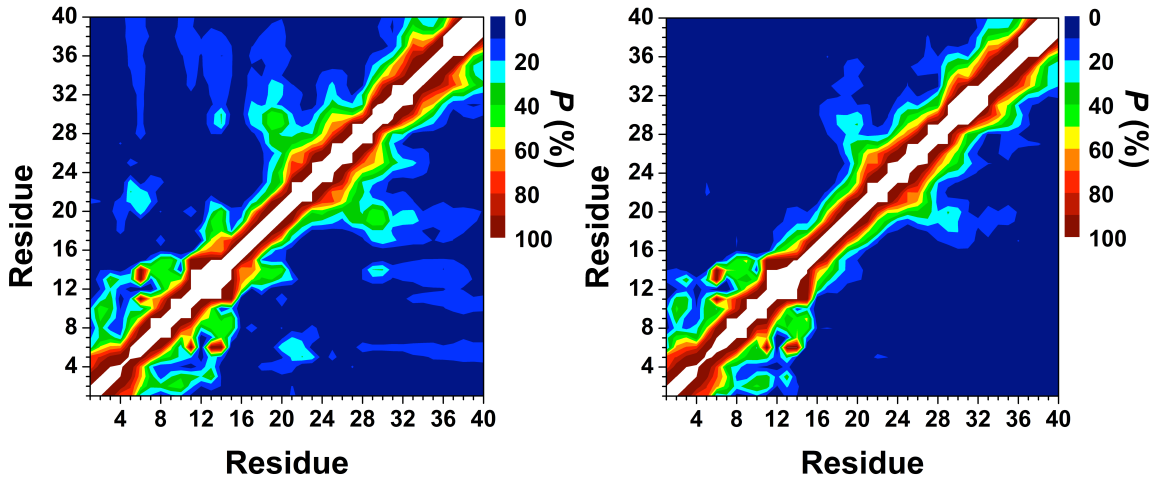

(a) (b)

**Figure S10.** Calculated intra-molecular metallopeptide interactions in the structures of Zn:Aβ40 located in (a) basin II and (b) basin III on the PMF surface (see Figures 2a and 2b); the color scale corresponds to the probability (*P*) of these interactions.

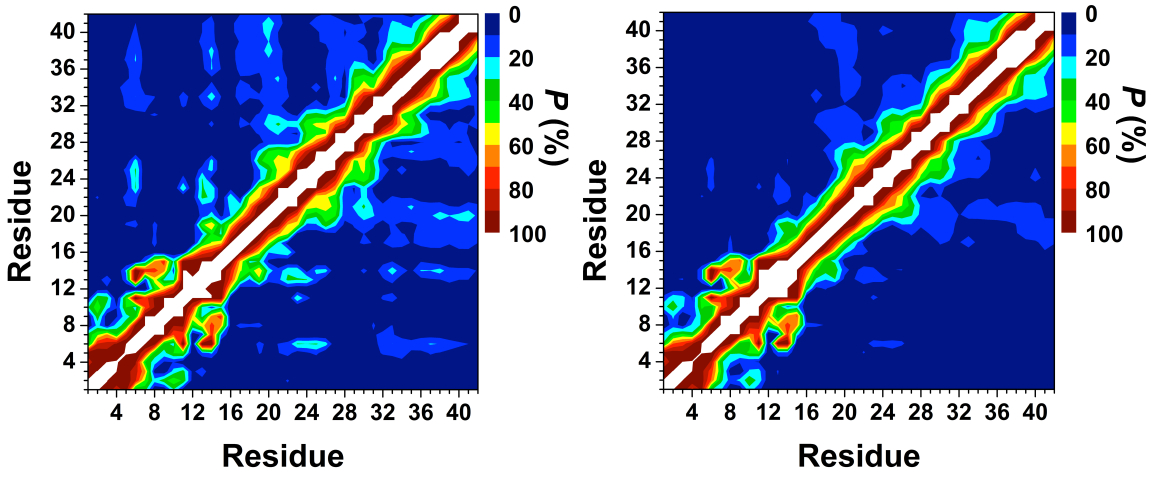


(a) (b)

**Figure S11.** Calculated intra-molecular metallopeptide interactions in the structures of Zn:Aβ42 located in (a) basin II and (b) basin III on the PMF surface (see Figures 2a and 2b); the color scale corresponds to the probability (*P*) of these interactions.

| Donor | Acceptor | R(C-N) (%) | | | | | | | | |
|---|---|---|---|---|---|---|---|---|---|---|
| | | I | | | II | | | III | | |
| | | ≤ 4 Å | ≤ 5 Å | ≤ 6 Å | ≤ 4 Å | ≤ 5 Å | ≤ 6 Å | ≤ 4 Å | ≤ 5 Å | ≤ 6 Å |
| **Arg5** | **Asp1** | 59.5 | 68.4 | 69.7 | 51.9 | 60.1 | 61.9 | 58.6 | 67.1 | 68.4 |
| **Arg5** | **Glu22** | 12.4 | 12.6 | 12.6 | 14.5 | 14.9 | 15.1 | 8.1 | 8.4 | 8.4 |
| **Lys28** | **Glu22** | 12.2 | 19.1 | 20.3 | 17.7 | 27.4 | 28.9 | 6.0 | 9.8 | 10.7 |
| **Arg5** | **Asp7** | 20.9 | 25.5 | 29.0 | 24.1 | 31.3 | 36.4 | 25.1 | 31.6 | 36.3 |
| **Arg5** | **Glu3** | 15.9 | 17.2 | 17.5 | 22.3 | 23.4 | 23.7 | 21.1 | 22.2 | 22.4 |
| **Arg5** | **Asp23** | 8.2 | 8.7 | 9.0 | 18.5 | 20.3 | 21.9 | 7.9 | 8.6 | 8.9 |
| **Lys28** | **Asp23** | 4.6 | 6.8 | 7.6 | 3.6 | 5.2 | 5.8 | 4.6 | 7.0 | 8.0 |
| **Lys16** | **Glu22** | 0.3 | 0.5 | 0.6 | 0.7 | 0.9 | 1.0 | 3.9 | 5.3 | 5.6 |

**Table S2.** The formed salt bridges in the structures of the Zn:Aβ40 metallopeptide located in basins I, II and III on the PMF surface; R(C-N) is the distance between the carboxylate C atom and the side-chain or N-terminus N atom.

| Donor | Acceptor | R(C-N) (%) | | | | | | | | |
|---|---|---|---|---|---|---|---|---|---|---|
| | | I | | | II | | | III | | |
| | | ≤ 4 Å | ≤ 5 Å | ≤ 6 Å | ≤ 4 Å | ≤ 5 Å | ≤ 6 Å | ≤ 4 Å | ≤ 5 Å | ≤ 6 Å |
| **Arg5** | **Asp1** | 86.1 | 98.3 | 98.8 | 82.8 | 92.2 | 93.5 | 74.6 | 84.9 | 86.0 |
| **Arg5** | **Glu22** | 13.5 | 13.7 | 13.7 | 15.9 | 16.2 | 16.2 | 15.0 | 15.2 | 15.2 |
| **Arg5** | **Asp7** | 29.8 | 32.3 | 33.8 | 26.3 | 30.7 | 33.7 | 16.4 | 19.7 | 22.1 |
| **Arg5** | **Glu3** | 1.0 | 1.0 | 1.0 | 6.4 | 7.1 | 7.4 | 10.6 | 11.9 | 12.5 |
| **Arg5** | **Asp23** | 30.5 | 30.6 | 30.9 | 4.1 | 4.1 | 4.2 | 2.1 | 2.2 | 2.2 |
| **Lys16** | **Glu22** | 25.3 | 34.8 | 36.5 | 19.1 | 25.1 | 26.1 | 8.6 | 11.4 | 12.0 |
| **Arg5** | **Glu11** | 1.8 | 8.2 | 35.7 | 2.4 | 7.1 | 16.7 | 1.3 | 4.9 | 11.7 |
| **Lys28** | **Asp23** | 3.9 | 5.4 | 6.0 | 2.9 | 4.6 | 5.6 | 5.0 | 7.5 | 8.8 |
| **Lys28** | **Glu22** | 0.8 | 1.2 | 1.3 | 2.7 | 4.4 | 5.0 | 1.7 | 2.8 | 3.2 |

**Table S3.** The formed salt bridges in the structures of the Zn:Aβ42 metallopeptide located in basins I, II, and III on the PMF surface; R(C-N) is the distance between the carboxylate C atom and the side-chain or N-terminus N atom.